Research Square

Preprints are preliminary reports that have not undergone peer review.
They should not be considered conclusive, used to inform clinical practice,
or referenced by the media as validated information.

Ocean thermal energy conversion and direct air capture as a pathway for meeting the Paris climate targets

Leslie Moffat
University of Victoria
Michael Eby
University of Victoria
Andrew John Weaver
weaver@uvic.ca

University of Victoria

Article

Keywords:

Posted Date: November 26th, 2026

DOI: https://doi.org/10.21203/rs.3.rs-11516834/v1

License: This work is licensed under a Creative Commons Attribution 4.0 International License.
Read Full License

Additional Declarations: No competing interests reported.

Abstract

Limiting warming to the Paris Agreement targets of 1.5°C and 2.0°C requires large-scale deployment of negative-emission technologies powered by low-carbon energy sources. Ocean thermal energy conversion (OTEC) and direct air carbon capture and storage (DACCS) offer a pathway for renewable-energy-powered atmospheric CO_2 removal and offshore geological sequestration. OTEC harnesses heat stored in the upper ocean from past greenhouse-gas warming to power CO_2 removal. Using the University of Victoria Earth System Climate Model, we identify viable deployment locations and model the conversion of OTEC power output to atmospheric CO_2 removal using two estimates of DACCS energy requirements. We then estimate the OTEC power required to remain below the Paris targets under a range of emissions pathways and transient climate response to emissions (TCRE) values.

We identify 120 suitable offshore sequestration reservoirs, including depleted oil and gas fields, saline aquifers, and basalt formations. Under present-day DACCS energy requirements, little additional deployment was required under Representative Concentration Pathway (RCP) 2.6, whereas neither temperature target could be achieved under RCP 8.5. Under intermediate-emission pathways (RCPs 4.5 and 6.0), feasibility depended strongly on mitigation timeline and TCRE. Required OTEC power increased with cumulative emissions, climate sensitivity, and shorter timelines to net zero. Improved DACCS efficiency substantially reduced deployment requirements and enabled some RCP 8.5 simulations to remain below the 2.0°C threshold. OTEC-powered DACCS could therefore contribute to climate stabilization but cannot substitute for rapid emissions reductions.

1 Introduction

In 2015, the Paris Agreement set the global goal of limiting the rise in global mean surface air temperature (GMSAT) to well below 2.0°C above pre-industrial temperatures, with additional efforts to limit the rise to 1.5°C. Consequences of exceeding these thresholds include decreased water availability, decreased agricultural and livestock production, increased infrastructure damage, and increased stressors to human health (IPCC 2023). Recent assessments estimated GMSAT has already risen 1.3°C by the end of 2024 (World Meteorological Organization 2025). The Intergovernmental Panel on Climate Change (IPCC) has identified the need for net negative emissions to remain below the 1.5°C and 2.0°C GMSAT thresholds (IPCC 2023). To remain below the thresholds with little to no overshoot by the end of the century, implementation of negative emission technologies will need to be accelerated by 2050 (IPCC 2023). Large-scale negative-emission technologies will require low-carbon energy sources to achieve this goal. A previously identified approach that fits this role is the coupling of Ocean Thermal Energy Conversion (OTEC) and Direct Air Carbon Capture and Storage (DACCS) (Olim et al. 2025). OTEC is a form of renewable energy (firm power) that relies on stored oceanic thermal energy. It is not limited by season or time of day and the vastness of the surface ocean provides immense untapped potential. Given that 90–91% of the excess heat accumulated in the Earth system from global warming is stored in the ocean (IPCC 2021), OTEC electricity could be used to power DACCS technology for CO_2 sequestration in offshore reservoirs with the added benefit of cooling the waters of the upper ocean.

Here, we aim to provide a first order estimate to the question, how much OTEC power production is required to support DACCS to meet the goals of the Paris Agreement to limit the rise in GMSAT?

1.1 Ocean Thermal Energy Conversion

OTEC harnesses solar energy stored in the vertical water column by using the thermal gradient to drive a heat engine. The heat from warm surface water evaporates a working fluid inside a heat exchanger. The working fluid in vapour form then passes through a turbine, expands, converting thermal energy to kinetic energy, and via a generator, electrical energy. The working fluid then proceeds to a second heat exchanger, where it is cooled by cold deep water and condenses back into a liquid before starting the cycle again. Using seawater as the working fluid is known as open-cycle while the choice of a refrigerant, such as ammonia, is a closed-cycle. Pipes and pumps are used to draw in warm surface water from the mixed layer. Cold deep water is pumped from approximately 1000 m depth; however, its exact depth depends on achieving a sufficient thermal gradient. After the warm and cold water have passed through their respective heat exchangers, the two are mixed and discharged. The discharge redistributes cold deep nutrient-rich water into the mixed layer, similar to artificial upwelling. However, artificial upwelling and OTEC mixing have been shown to result in dissimilar ocean chemistry profiles, while artificial upwelling only temporarily cool the ocean surface (Nickoloff et al. 2025b). In a closed-cycle, the recirculating working fluid circuit and the seawater intake/discharge circuit are kept separate and do not mix. As a result, non-seawater working fluids are not released into the surrounding environment. Net power generation is dependent on the temperature difference between warm and cold waters. A difference of 18°C between the warm surface water and cold deep water is widely suggested as the minimum gradient to merit energy extraction using OTEC technology given the low efficiency of applied heat engines (Nihous 2007; Rajagopalan and Nihous 2013). Fortunately, this gradient exists in the top 1000 m of the water column across a large portion of the world's ocean and establishes the tropics (between 23°N and 23°S) as the optimal location for OTEC implementation (Ocean Energy System 2021).While OTEC has not yet reached the large-scale implementation phase, interest in OTEC technology has continued to grow alongside increasing demand for renewable energy. It is widely suggested that decommissioned oil and gas floating structures be repurposed to house OTEC technology, to reduce initial building costs (Aresti et al. 2023; Ocean Energy System 2021). Oil and gas infrastructure has undergone decades of development and has proven durable, which, if repurposed, will accelerate the practical application of OTEC facilities while creating a transitional path away from reliance on fossil fuels (Ocean Energy System 2021).

1.2 Direct Air Capture and CO_2 Sequestration

The IPCC has identified that net negative global emissions are necessary to stay below a 2.0°C rise in GMSAT above pre-industrial temperatures, and CO_2 sequestration will need to exist on the order of 100 to 1000 $PgCO_2$ (27 to 273 PgC) by the end of the century to remain below the 1.5°C threshold (IPCC 2018). DACCS is the process of capturing atmospheric CO_2, converting it to supercritical liquid form, transporting it, and injecting it into land or offshore reservoirs where it is prevented from returning to the

atmosphere. As of 2022, total global CO_2 sequestration capacity was only ~ 0.01 $MtCO_2$/yr from direct air capture facilities (International Energy Agency 2022).

One of the primary types of filtering materials used to isolate CO_2 from ambient air is liquid solvents. Solvents can be reused after the CO_2 is released, so the process can operate continuously; however, it does require water and additional energy input to regenerate the solvent (International Energy Agency 2022). Liquid solvent direct air capture is less energy intensive but more costly than other forms, making it suitable for large-scale capture.

Once removed from the atmosphere, CO_2 must be securely stored. Three types of offshore reservoirs have been identified as suitable for long-term geological CO_2 sequestration: depleted oil and gas fields, saline aquifers, and basalt formations. Appropriate CO_2 injection infrastructure already exists and is in place for many oil and gas fields, given the extent of the oil extraction industry. The cost of storage in depleted oil and gas fields is projected to be lower by reusing oil and gas extraction technology (Maroto-Valer 2010).

1.3 Transient Climate Response to Emissions

Numerous studies have identified a near-linear relationship between the rise in GMSAT and cumulative CO_2 emissions (Weaver et al. 2008; Gregory et al. 2009; Matthews et al. 2009; Zickfeld et al. 2009; IPCC 2021). This relationship is quantified by the Transient Climate Response to Emissions (TCRE), which describes the amount of warming in degrees Celsius per 1000 PgC of cumulative carbon emitted. The near-constant nature of TCRE is thought to arise from compensating processes involving the logarithmic decrease in sensitivity of radiative forcing to atmospheric CO_2 and the declining efficiency of ocean heat and carbon uptake at higher CO_2 concentrations (Gregory et al. 2009; Matthews et al. 2009; MacDougall and Friedlingstein 2015). Together, these opposing effects produce an approximately linear warming response to cumulative CO_2 emissions.

Studies suggest that TCRE is largely independent of emissions pathway and depends primarily on cumulative emissions rather than the historical rate of emissions (MacDougall et al. 2017; Seshadri 2017). However, this path independence may weaken at extremely high or low emissions rates, where assumptions regarding terrestrial carbon storage, climate feedbacks, and ocean heat uptake efficacy become less valid (MacDougall et al. 2017; Seshadri 2017). Exceeding a warming threshold, followed by a period of net-negative emissions sufficient to return cumulative emissions below that threshold, is referred to as an overshoot scenario. Although sufficient CO_2 sequestration may ultimately stabilize GMSAT below a given threshold, it does not guarantee that warming will not initially exceed that threshold. Overshoot, therefore, carries additional climate risks regardless of the eventual equilibrium state. Furthermore, previous studies suggest that a decade to multi-decadal lag may exist between CO_2 emissions and the peak of the associated temperature response, depending on the magnitude of the emissions pulse (Ricke and Caldeira 2014; Zickfeld and Herrington 2015). As a result, warming may continue even after net-zero or net-negative emissions are achieved.

The IPCC Sixth Assessment Report estimated the TCRE to be in the likely range from 1.0 to 2.3°C per 1000 PgC emitted, with a best estimate of 1.65°C per 1000 PgC (IPCC 2021). Much of the uncertainty in TCRE is associated with the ocean carbon sink, which strongly influences the airborne fraction of atmospheric CO_2 (Jones and Friedlingstein 2020; Katavouta et al. 2018; MacDougall et al. 2017). TCRE can therefore be used to estimate the remaining carbon budget associated with a given warming threshold. GMSAT is estimated to have already risen approximately 1.3°C above pre-industrial temperatures (1850–1900) by 2024 (World Meteorological Organization 2025), leaving only an additional 0.2°C and 0.7°C of warming before the 1.5°C and 2.0°C thresholds are reached, respectively.

2 Methodology

2.1 Model description

We use the University of Victoria Earth System Climate Model (UVic ESCM) version 2.9. The UVic ESCM is a coupled, intermediate complexity global climate model (Weaver et al. 2001). The model consists of a spherical grid with a zonal resolution of 3.6°, a meridional resolution of 1.8°, and 19 vertical ocean levels (Weaver et al. 2001). The UVic ESCM includes a three-dimensional ocean general circulation model, a two-dimensional energy-moisture balance atmospheric model, a thermodynamic-dynamic sea-ice model, and a thermomechanical land-ice model (Weaver et al. 2001). The ocean general circulation model comprises the Geophysical Fluid Dynamics Laboratory Modular Ocean Model version 2.2 based on the Navier-Stokes equations under the Boussinesq and hydrostatic approximations (Pacanowski 1996). The atmospheric model, with dynamical feedbacks, is based on the Fanning and Weaver (1996) energy-moisture balance model, which utilizes vertically integrated thermodynamic energy balance equations and a parameterization of atmospheric heat and moisture transport through Fickian diffusion (Weaver et al. 2001). The radiative forcing due to changes in atmospheric CO_2 concentration is represented by a modification of the planetary longwave radiative flux (Weaver et al. 2001). The thermodynamic-dynamic sea-ice model also includes an elastic-viscous-plastic rheology to represent dynamics (Weaver et al. 2001). A quantitative evaluation of the UVic ESCM climatology can be found in Weaver et al. (2001).

Here, a parameterization representing OTEC power production and mixing is incorporated following Nickoloff et al. (2025a, b). The OTEC power production represents a closed-cycle with an unspecified non-seawater working fluid. OTEC facilities are presumed to be autonomous floating platforms capable of deployment in the model's ocean grid cells. Sub-grid-scale mixing is used to model OTEC intake and discharge before being spread across the larger grid cell. The cold-water intake is parametrized by a sink with a pipe radius of 10 m at a depth of 1100 m. The warm water intake sink draws in water with the same pipe diameter at the surface. Water properties from the two intakes are mixed and then discharged at a near-surface depth of approximately 20 m. As the discharge is denser than the surrounding water, it is mixed downwards to a depth of neutral buoyancy. During this downward mixing, the plume entrains surrounding water, thereby lowering its density and reducing its depth of penetration. This entrainment is parameterized by ten concentric vertical columns, each 50 m thick, over a cross-sectional area of 500 m,

where the outermost ring represents the region of discharge producing the highest amount of entrainment and the lowest amount of vertical penetration. The near-field radius of horizontal mixing, from studies by Rocheleau and Grandelli (2011) and Rodríguez Buño (2013), was used as the radius of entrainment. The discharge volume is distributed linearly, with the maximum occurring at the center of the discharge area and the minimum (zero) at the outer edge. This results in the depth of penetration also decreasing, as the distance from the centre of discharge increases. Vertical mixing is calculated for each of the ten columns separately and then mixed laterally at all depths, weighted by the surface area relative to the surface area of the grid cell.

The discharge of cold deep water into the mixed layer produced by the OTEC cycle is often compared to artificial upwelling, which has been suggested to strengthen the carbon flux from the atmosphere to the ocean and result in net CO_2 removal from the atmosphere (Ocean Energy System 2021). While this effect induced by OTEC deployment has been previously modelled (Nickoloff et al. 2025b), the focus of this research is to quantify the removal of atmospheric CO_2 by way of OTEC powered DACCS, not passive the flow of CO_2 from the atmosphere to the ocean.

The power production simulated by the model is consistent with closed-cycle OTEC behaviour. The theoretical net power output ($\mathrm{P_{net}}$) in watts can be expressed as Eq. 1 (Nickoloff et al. 2025a).

$$P_{net} = \omega_{cw} \rho\, c_p \epsilon_{tg} \left(\frac{9}{80} \frac{(\Delta T)^2}{T} - \frac{9}{200} \right) \text{(Eq. 1)}$$

The input variables are: 1) warm water intake temperature (T in K); 2) temperature gradient between cold and warm water intakes (ΔT in K); 3) cold water volume flow rate (ω_{cw} in $m^3 s^{-1}$); 4) mean reference seawater density (ρ =1025 $kg \cdot m^{-3}$); 5) specific heat ($c_p = 4000$ $J \cdot kg^{-1} \cdot K^{-1}$); 6) OTEC combined turbo-generator efficiency (ϵ_{tg}). Reference variables used in calculation coefficients do not imply constant variables present in the model and are only used here for the purpose of single grid-cell power calculations.

The velocity flow was set to 1 $m \cdot s^{-1}$ to achieve a volume flow rate of $\omega_{cw} = 314$ $m^3 \cdot s^{-1}$. As such, each OTEC facility produces roughly 100 MW of power. The turbo-generator efficiency in *Eq. 1* was set to ϵ_{tg} = 0.75 (Nickoloff et al. 2025a). As in Nickoloff et al. (2025a), the main constraint to facility power production is the magnitude of the vertical ocean thermal gradient. Here, we determined OTEC facility locations by identifying regions with the highest potential power production. This was accomplished by ranking the ocean model grid cells by the magnitude of the thermal gradient between the warm- and cold-water intake depths. Facilities were continually placed until either the target global power was produced or there were no longer any viable deployment locations. Potential deployment locations were identified if a facility's potential net power production exceeded a minimum threshold of 75 MW. The purpose of this threshold is to exclude poorly performing deployment. Multiple facilities could be placed in a single grid cell; however, this reduced the power production of each facility since each deployment further depleted the thermal gradient. To minimize overcrowding, thermal gradient depletion, and effluent

discharge from a facility being consumed by a facility downstream, a minimum area of 200 km^2 was set for each facility. This criterion does not guarantee, but is shown to prevent, interference between facilities (Nickoloff 2025a). Facilities were removed when their power production fell below 75 MW due to the depletion of the vertical ocean temperature gradient.

2.2 Experimental Configuration

Considerable research has examined the extent and capacity of offshore CO_2 sequestration reservoirs at both global and regional scales. Offshore basalt formations identified by Goldberg and Slagle (2009) as suitable for CO_2 sequestration, based on formation mechanics, age, proximity to plate boundaries, overlying sediment thickness, and water depth, were selected as potential OTEC deployment sites. Basalt formations were additionally required to possess a minimum sequestration capacity of 5 $PgCO_2$ (1.4 PgC), as smaller reservoirs were considered impractical for large-scale deployment (Planke et al. 2021). Suitable offshore depleted oil and gas fields and saline aquifers were also selected from the Oil and Gas Climate Initiative's Cycle 4 CO_2 Storage Resource Catalogue (Oil and Gas Climate Initiative 2023). All candidate reservoirs were subsequently filtered to include only regions where the UVic ESCM simulated an initial vertical thermal gradient of at least 18°C. An ocean mask was then applied to restrict OTEC deployment to grid cells containing suitable offshore CO_2 sequestration reservoirs. A complete list of candidate sites and details of map allocation are provided in Table A1 in the Supplementary Material.

All model integrations began from a 10,000-year equilibrium spin-up of the UVic ESCM forced only by seasonally varying conditions representative of 850 CE. The spin-up procedure is implemented to allow the ocean and carbon reservoirs to approach equilibrium under seasonally varying forcings and avoid spurious drift during the subsequent experiments. Initial conditions for the year 2000 were obtained by integrating the model from 1850 to 2000 with transient historical forcings following Eby et al. (2009). From 2000 to 2300, the model was forced by each of the extended 2.6, 4.5, 6.0, and 8.5 Representative Concentration Pathway (RCP) scenarios as detailed in Zickfeld et al. (2013). Beyond 2300, annual mean forcing was held constant while retaining seasonal variability (Zickfeld et al. 2013). Control integrations without OTEC deployment or CO_2 sequestration were extended to 2500 and used as baseline comparisons for subsequent OTEC simulations. For each RCP scenario, model CO_2 emissions were diagnosed and used to force the coupled deployment experiments. A series of sensitivity experiments was conducted to determine the cold-water intake depth and deployment pathway that optimized OTEC power production. OTEC deployment is typically limited to ocean depths greater than 1000 m, where sufficiently cold water exists to maintain a viable thermal gradient. Sensitivity tests, therefore, examined whether allowing deployment in shallower regions that still maintained thermal gradients exceeding 18°C and net power production greater than 75 MW altered the global deployment potential. Expanding the allowable intake depth range produced only minor increases in global OTEC-DACCS potential (Moffat 2026). Additional experiments examined the influence of deployment pathway shape using raised-cosine, linear, and exponential deployment curves. Deviations from the default raised-cosine deployment pathway produced negligible differences (Moffat 2026).

To estimate the effects of OTEC-driven DACCS on GMSAT, TCRE was used to project the temperature response to cumulative CO_2 emissions. Remaining allowable emissions before exceeding the 1.5°C and 2.0°C GMSAT thresholds were calculated and used to determine the remaining carbon budgets associated with an additional 0.2°C and 0.7°C of warming beyond 2024. Budgets were estimated using TCRE values of 1.0°C, 1.65°C, 2.0°C, and 2.3°C per 1000 PgC emitted. The values of 1.0°C, 1.65°C, and 2.3°C correspond to the minimum, best-estimate, and maximum TCRE estimates from the IPCC Sixth Assessment Report (IPCC 2021), while 2.0°C per 1000 PgC approximates the effective TCRE of the UVic ESCM (Eby et al. 2013; Matthews et al. 2009; Zickfeld et al. 2013). These allowable carbon budgets were subsequently used to determine when sufficient OTEC-driven DACCS capacity was achieved to remain below the GMSAT thresholds.

Carbon dioxide sequestration was represented as a negative emission of anthropogenic CO_2. Following Olim et al. (2025), two DACCS energy-demand scenarios were considered: an estimate of current technological standards, namely 1921 kWh per tonne of CO_2 sequestered (scenario OTEC-HIGH), and an optimistic future estimate of 366 kWh per tonne of CO_2 sequestered (scenario OTEC-LOW; Keith et al. 2018). OTEC supplied the energy allocated to the modelled capture process under each assumed energy-demand case. For simplicity, the RCP-derived baseline emissions with OTEC and DACCS removal will hereafter be referred to as solely as RCP scenarios. All integrations included the expanded shallow-water deployment regions and followed the raised-cosine deployment pathway for RCPs 2.6, 4.5, 6.0, and 8.5. Simulations included target peak OTEC power production ranging from 1 to 10 TW for OTEC-HIGH conditions and from 0.1 to 6 TW for OTEC-LOW conditions, with all deployments peaking in the year 2100. Coupled deployment integrations began in the year 2000 and initiated deployment in 2030. Target peak power production was projected for the 2100 and then held constant until 2500, unless unsustainable due to gradient depletion. A full list of integrations and their adjusted parameters can be found in Moffat (2026).

The OTEC power required to remain below the GMSAT thresholds was estimated from projected cumulative CO_2 emissions for the years 2100, 2300, and 2500, representing different assessment horizons. Cumulative emissions were compared with threshold carbon budgets as a function of peak OTEC power production. Where the target peak power was not fully achieved, the realized peak power was used instead. For each combination of end year, TCRE value, GMSAT threshold, and sequestration-energy scenario, linear interpolation between bounding simulations was used to estimate the minimum peak power required to remain below the temperature threshold. No extrapolation beyond the maximum simulated power level was performed when sequestration remained insufficient to avoid threshold exceedance.

Finally, the interpolated peak-power estimates were used to determine the corresponding number of required OTEC facilities for each TCRE value, RCP, GMSAT threshold, and timeline to remain below the GMSAT threshold. All results are summarized in Tables A2-A5 in the Supplementary Material. To

conclude, a cost analysis was undertaken following the method outlined in Olim et al. (2025), using a combination of capital costs per facility and ongoing expenses to sequester CO_2.

3 Results and Discussion

3.1 Identification of Sequestration Reservoirs

Offshore CO_2 sequestration reservoirs were identified and classified as depleted oil and gas fields, saline aquifers, or basalt formations. Figure 1 illustrates regions with sufficient vertical thermal gradients to support OTEC power production by 2030, together with viable offshore sequestration reservoirs. The strongest thermal gradients occur within the equatorial western Pacific Ocean, particularly the Pacific Warm Pool. The Ontong Java Plateau, a large basalt formation located near the thermal-gradient maximum, was identified as one of the most favourable sequestration sites.

In total, 120 reservoirs were identified as suitable for coupled OTEC deployment and CO_2 storage, including 47 depleted oil and gas fields, 65 saline aquifers, and 8 basalt formations (see Table A1). A complete list of reservoirs is provided in the Supplementary Material. The identified reservoirs are candidate storage opportunities, and do not constitute a fleet of injection facilities or existing infrastructure. Injection rates and pressure management of reservoirs remain to be assessed in order to confirm their readiness for operation. Estimated reservoir storage capacities were compared with the quantity of carbon sequestered in subsequent model integrations, and no scenario exceeded the available storage capacity of the identified reservoirs.

Figure 1: Map identifying the potential OTEC/DACCS deployment sites. The region with an adequate thermal gradient of 18°C or greater is also contoured. Potential carbon sequestration reservoirs are indicated by dots: saline aquifers (purple); depleted oil and gas fields (green); and basalt formation regions (red). Sites across all categories of water depths are included. The region with an adequate thermal gradient of 18°C or greater is represented as a contour plot.

3.2 Model Temperature Response to CO_2 Emissions

To evaluate the feasibility of using coupled OTEC and DACCS deployment to remain below the GMSAT thresholds, the TCRE framework was used to estimate the remaining carbon budgets. The applicability of TCRE within the UVic ESCM was assessed by comparing changes in GMSAT with cumulative carbon emissions (Figure 2). When the emissions axis is scaled using the model's approximate TCRE value of 2.0°C per 1000 PgC, the GMSAT anomaly and cumulative emissions should, in principle, follow similar trajectories, particularly after 2300 when emissions are low.

Across all RCPs and deployment scenarios, the GMSAT response lagged cumulative emissions. This delayed warming response is consistent with previous studies showing that peak warming can occur years to decades after a CO_2 emissions pulse because of the thermal inertia of the climate system (Ricke and Caldeira 2014; Zickfeld and Herrington 2015). The lag was most pronounced under RCP 8.5

relative to RCPs 2.6, 4.5, and 6.0, suggesting that the response timescale increases with the magnitude of cumulative emissions.

Figure 2: Year 2025 to year 2500 change in GMSAT (°C; orange) and cumulative emissions (PgC; blue) since the pre-industrial era. Trajectories are shown for integrations under RCP 2.6 (solid), RCP 4.5 (dashed), RCP 6.0 (dotted), and RCP 8.5 (dash-dotted). Horizontal black lines represent the observed offset between the change in GMSAT and cumulative emissions from the pre-industrial era to the year 2025 (Friedlingstein et al. 2025; World Meteorological Organization 2025). **a)** trajectories for control scenarios without coupled OTEC and DACCS deployment; **b)** trajectories for integrations with 2 TW of target peak power production and the OTEC-HIGH condition for sequestration energy. Vertical axes are scaled to represent a TCRE value of 2.0°C per 1000 PgC.

For RCPs 2.6, 4.5, and 6.0, the trajectories of GMSAT anomaly and cumulative emissions tracked closely, whereas larger discrepancies emerged under RCP 8.5. This behaviour suggests that the effective TCRE of the model may not remain constant at high atmospheric CO_2 concentrations and warming levels (MacDougall et al. 2017; Seshadri 2017). In particular, the divergence in trends under RCP 8.5 suggests that the effective TCRE of the UVic ESCM is lower than 2.0°C per 1000 PgC under extreme warming scenarios. This is most evident in the control integrations (Figure 2a), where the effective TCRE for RCP 8.5 appears closer to 1.7°C per 1000 PgC, while RCPs 2.6, 4.5, and 6.0 remain more consistent with values near or slightly above 2.0°C per 1000 PgC. These results suggest that the assumption of a single TCRE value becomes less robust at high levels of warming and atmospheric CO_2.

Equilibrium relationships between cumulative emissions and temperature were also more difficult to assess under RCP 8.5 in scenarios with large emission reductions, as GMSAT had insufficient time to fully respond to declining emissions. This behaviour is illustrated in the 2 TW deployment scenarios shown in Figure 2b, where cumulative emissions under RCP 8.5 began to decline after 2200 while temperatures continued to increase slightly. In contrast, temperature and cumulative-emissions trajectories remained in closer agreement for RCPs 2.6, 4.5, and 6.0. These results suggest that a TCRE value of approximately 2.0°C per 1000 PgC provides a reasonable approximation for the UVic ESCM under moderate-emissions scenarios.

Overshoot followed by declining cumulative emissions and delayed temperature stabilization occurred frequently across the integrations. Despite the additional uncertainty introduced under overshoot conditions, the close agreement between temperature and cumulative-emissions anomalies for RCPs 2.6, 4.5, and 6.0 indicates that TCRE remains a useful framework for estimating the remaining carbon budgets associated with the 1.5°C and 2.0°C GMSAT thresholds. The analysis, therefore, focuses primarily on RCPs 4.5 and 6.0, as RCP 2.6 already assumes substantial negative emissions that could, in part, be supplied by OTEC-driven DACCS deployment.

3.3 Power Targets

Estimated OTEC power production required to sequester sufficient CO_2 to remain below the GMSAT thresholds across the four RCP and TCRE scenarios is provided in Tables A2 and A3. The highest confidence is associated with simulations assuming a TCRE value of 2.0°C per 1000 PgC, as this most closely matches the effective TCRE of the UVic ESCM. Because the model's TCRE directly influences projected warming, it also affects OTEC efficiency, deployment extent, and the interpolated peak-power requirements. Consequently, uncertainty increases as the prescribed TCRE diverges from the model's effective value.

3.3.1 Present-day estimates of sequestration potential

Table 1 summarizes the OTEC-HIGH scenarios, which assume a DACCS energy requirement of 1921 kWh per tonne of CO_2 sequestered, across TCRE values ranging from 1.0 to 2.3°C per 1000 PgC and assessment horizons. Under OTEC-HIGH conditions, neither the 1.5°C nor 2.0°C GMSAT thresholds could be achieved under RCP 8.5, as insufficient OTEC power was available to sequester enough CO_2 to offset warming. These results suggest that coupled OTEC and DACCS deployment alone would be insufficient to provide the negative emissions required under RCP 8.5.

In contrast, little additional power was required to remain below either threshold under RCP 2.6. However, RCP 2.6 already assumes substantial negative emissions, which could, in part, be supplied by OTEC-driven DACCS deployment.

RCP	2100		2300		2500	
	1.5°C	2.0°C	1.5°C	2.0°C	1.5°C	2.0°C
2.6	≤ 0.1	0.0	<< 0.1	0.0	<< 0.1	0.0
4.5	—	0.0-5.0	1.9-2.3	0.2-1.5	1.2-1.4	0.3-1.0
6.0	—	3.83- —	4.5-5.2	2.4-3.9	2.4-2.7	1.5-2.3
8.5	—	—	—	—	—	—

Table 1: Target peak power (TW) required in year 2100 to remain below the indicated GMSAT threshold of either 1.5°C or 2.0°C above pre-industrial temperatures for CO_2 emissions from RCP 2.6, RCP 4.5, RCP 6.0, and RCP 8.5. The estimates are from OTEC-HIGH scenarios with a sequestration energy of 1921 kWh per tonne of CO_2 sequestered. Target peak powers are given for deadlines to remain below the GMSAT thresholds of 2100, 2300, and 2500. Each estimate range includes projections for scenarios for TCRE values of 1.0, 1.65, 2.0, and 2.3 °C per 1000 PgC.

For the 2100 timeline, neither RCP 4.5 nor RCP 6.0 remained below the 1.5°C GMSAT threshold. In all scenarios, insufficient OTEC power was available to sequester enough CO_2 to offset post-overshoot warming. Given current global emissions trajectories and the increasing improbability of following an

RCP 2.6-like pathway, it appears unlikely that coupled OTEC and DACCS deployment, using current DACCS technology, could prevent surpassing the 1.5°C threshold by 2100.

For the 2.0°C threshold under the 2100 timeline, only RCP 4.5 produced sufficient CO_2 sequestration across the full TCRE range. Required OTEC power production under RCP 4.5 ranged from 0 to 5.0 TW, depending on the assumed TCRE value, representing one of the broadest ranges identified in the analysis. Under RCP 6.0, sufficient sequestration was achieved only for the lowest TCRE value of 1.0°C per 1000 PgC. Given the insufficient sequestration under RCP 6.0 and the substantial uncertainty under RCP 4.5, it appears unlikely that OTEC deployment coupled with current DACCS technology alone could maintain warming below the 2.0°C threshold by 2100.

In contrast, timelines extending to 2300 and 2500 produced sufficient power generation under both RCP 4.5 and RCP 6.0 to remain below the GMSAT thresholds across the full TCRE range. To remain below the 2.0°C threshold, RCP 4.5 required between 0.2–1.5 TW and 0.3–1.0 TW of OTEC power production for the 2300 and 2500 timelines, respectively. Equivalent requirements under RCP 6.0 ranged from 2.4–3.9 TW and 1.5–2.3 TW. These results suggest that coupled OTEC and DACCS deployment could contribute meaningfully to long-term climate stabilization under moderate-emission scenarios, provided sufficiently long mitigation timelines are available.

Across all OTEC-HIGH scenarios, required power production increased systematically with increasing TCRE, increasing emissions pathway, and shorter mitigation timelines. Higher TCRE values produced greater warming per unit carbon emitted, while higher RCPs incorporated larger cumulative emissions and associated warming. Shorter timelines also required greater peak power production because equivalent carbon sequestration had to occur over a reduced time interval. Together, these results demonstrate that required OTEC deployment increases with increasing climate sensitivity, cumulative emissions, and the urgency of mitigation.

3.3.2 Future estimates of sequestration potential

Table 2 summarizes the OTEC-LOW scenarios, which assume a DACCS energy requirement of 366 kWh per tonne of CO_2 sequestered, for timelines ending in 2100, 2300, and 2500. The reported power ranges reflect the full range of TCRE values considered. Similar to the OTEC-HIGH scenarios, little additional power was required to remain below either GMSAT threshold under RCP 2.6.

Unlike the OTEC-HIGH cases, however, the OTEC-LOW scenarios produced sufficient CO_2 sequestration to remain below the thresholds under some RCP 8.5 conditions. For the 2300 and 2500 timelines, sufficient OTEC power production was achieved to remain below both GMSAT thresholds. Under the 2100 timeline, enough power was available to remain below the 2.0°C threshold across the full TCRE range, although insufficient power was produced to prevent surpassing the 1.5°C threshold.

Relative to the OTEC-HIGH scenarios, these results suggest that substantial improvements in DACCS efficiency are required before coupled OTEC and DACCS deployment could contribute meaningfully

under high-emission pathways such as RCP 8.5. Current DACCS energy demands appear too large for OTEC alone to provide sufficient negative emissions to remain below the GMSAT thresholds under these scenarios.

RCP	2100		2300		2500	
	1.5°C	2.0°C	1.5°C	2.0°C	1.5°C	2.0°C
2.6	<< 0.1	0.0	<< 0.1	0.0	<< 0.1	0.0
4.5	1.5-2.0	0.0-1.0	0.4	0.0-0.3	0.2-0.3	0.0-0.2
6.0	3.0-3.5	0.7-2.5	0.8-0.9	0.5-0.7	0.5	0.3-0.4
8.5	5.2- —	3.2-5.0	2.6-2.7	2.3-2.6	1.5-1.6	1.3-1.5

Table 2: Target peak power (TW) required in year 2100 to remain below the indicated GMSAT threshold of either 1.5°C or 2.0°C above pre-industrial temperatures for CO_2 emissions from RCP 2.6, RCP 4.5, RCP 6.0, and RCP 8.5. The estimates are from OTEC-LOW scenarios with a sequestration energy of 366 kWh per tonne of CO_2 sequestered. Target peak powers are given for deadlines to remain below the GMSAT thresholds of 2100, 2300, and 2500. Each estimate range includes projections for scenarios for TCRE values of 1.0, 1.65, 2.0, and 2.3 °C per 1000 PgC.

For the 2300 and 2500 timelines, RCP 4.5 and 6.0 produced trends similar to the OTEC-HIGH scenarios but required substantially lower power production to remain below the GMSAT thresholds. Under RCP 4.5, no additional OTEC deployment was required to remain below the 2.0°C threshold for the lowest TCRE value of 1.0°C per 1000 PgC. Across the full TCRE range, RCP 4.5 required between 0–0.3 TW and 0–0.2 TW of OTEC power production for the 2300 and 2500 timelines, respectively. Equivalent requirements under RCP 6.0 ranged from 0.5–0.7 TW and 0.3–0.4 TW.

Overall, the OTEC-LOW scenarios produced trends similar to the OTEC-HIGH simulations but required substantially less power to achieve equivalent CO_2 sequestration. As with the OTEC-HIGH cases, required power production increased systematically with increasing TCRE, increasing emissions pathway, and shorter mitigation timelines.

3.4 Cost Analysis

High implementation costs are widely considered one of the primary barriers to large-scale OTEC deployment, reflecting the early developmental stage of the industry. Limited awareness of OTEC technology has also constrained investment and policy support. Current estimates for the construction and operation of OTEC facilities remain high, although uncertainties are substantial relative to more established renewable and non-renewable energy technologies (Shen et al. 2020; Ocean Energy System 2021). However, costs are expected to decline as the technology matures and deployment scales increase (Langer et al. 2020). Additional economic incentives, including carbon credits, subsidies, and

tax reductions, may further improve feasibility given the potential emissions reductions associated with OTEC deployment (Ocean Energy System 2021).

Following the cost-analysis framework of Olim et al. (2025), total deployment costs for coupled OTEC and DACCS systems were estimated for RCPs 4.5 and 6.0 using the mean projected TCRE value of 1.65°C per 1000 PgC and timelines extending to 2300 and 2500 (Table 3). Total costs combined estimated expenditures per OTEC facility and ongoing offshore CO_2 storage costs. OTEC expenditures include upfront costs as well as operations expenses which include factors such as maintenance, replacement of components, and personnel monitoring. OTEC costs as estimated to range from 5,000–15,000 USD_{2018} per kW of facility power production capacity (7,478–22,433 USD_{2025} per kW; Kempener and Neumann 2014; Muralidharan 2012) with ongoing offshore CO_2 storage costs of approximately 35 USD_{2023} (38 USD_{2025}) per tonne of CO_2 stored (IEA 2022). Estimated facility counts for each scenario are provided in the Supplementary Material. Repurposing existing oil and gas infrastructure is expected to reduce OTEC costs, however, given an inventory of existing accessible infrastructure is not available, no reductions were applied.

Scenarios under RCP 6.0 required substantially greater OTEC deployment and CO_2 sequestration than those under RCP 4.5, resulting in correspondingly higher total costs. Estimated costs under RCP 4.5 ranged from 50.0–58.4 trillion USD_{2025} and 60.0–66.3 trillion USD_{2025} for the 2300 and 2500 timelines, respectively. Equivalent costs under RCP 6.0 ranged from 150–180 trillion USD_{2025} and 160–175 trillion USD_{2025}.

RCP	Number of Plants Required		Carbon Sequestered (PgC)		Estimated Cost (trillions of USD_{2025})	
	2300	2500	2300	2500	2300	2500
4.5	5,578	3,727	330	417	50.0-58.4	60-66.3
6.0	19,676	10,246	976	1,093	150-180	160-175

Table 3: Projected costs (USD2025) of coupled OTEC and DACCS deployment for scenarios under RCP 4.5 and RCP 6.0. Estimates are given for scenarios with a TCRE value of 1.65°C per 1000 PgC. Columns 2 and 3 list the number of plants used to calculate the total cost. Columns 4 and 5 list the total carbon stored (PgC) in each scenario. This, in turn, is used to calculate the ongoing costs of DACCS.

In general, the 2500 timelines involved greater cumulative CO_2 sequestration but fewer deployed facilities than the corresponding 2300 scenarios. Because CO_2 sequestration costs ultimately exceeded OTEC facility expenditures, scenarios extending to 2500 produced higher overall costs than those ending in 2300. These results suggest that earlier implementation of coupled OTEC and DACCS deployment could reduce total project costs since the sooner net-zero is reached the less overall CO_2 has to be sequestered.

3.5 Environmental safety

Numerous environmental concerns have been identified in relation to coupled OTEC and DACCS deployment. The dynamics of deep ocean ecosystems located at depths suggested for cold water intake pipes are not well understood, and deep ocean species are highly susceptible to changes in temperature, salinity, pH, etc. (Hammar et al., 2017). The infrastructure of offshore and floating OTEC facilities could act as fish aggregating devices, attracting marine fauna and potentially creating artificial reef communities (Comfort & Vega, 2011; Hammar et al., 2017). This introduction of hard substrates is shown to alter the foraging patterns of marine mammals, which consequently affects the entire food chain (Russell et al., 2014). High mortality rates are associated with entrainment and impingement of small marine organisms by the large flow rates of intake pipes (Comfort & Vega, 2011; Hammar et al., 2017). Hammar et al. (2017) identified two categories of hazardous materials, toxic metals and halocarbons and halogens, that could leak into surrounding waters during OTEC activity (Hammar et al., 2017). Both classes of materials could cause irreparable damage to nearby ecosystems or leave them vulnerable to additional pressures (Aresti et al., 2023; Hammar et al., 2017). Furthermore, the relocation of large masses of deep ocean water to the photic zone will affect primary productivity given the increased surface concentrations of ordinarily limited macronutrients and trace metals (Aresti et al., 2023; Comfort & Vega, 2011; Hammar et al., 2017). OTEC induced artificial upwelling in oligotrophic waters would alter the composition of phytoplankton communities.

These potential effects are challenged by the fact that jurisdictional boundaries rarely align with the scale of OTEC effects, which renders accurate assessments of potential environmental impacts at proposed facility locations difficult. OTEC effects comprise physical, chemical, and biological environmental changes, which have the potential to act non-linearly, producing a disturbance larger than the sum of their parts (Hammar et al., 2017). As a result, it is sensible to conduct site-specific field assessments of significant parameters such as temperature, salinity, pH, etc., at potential OTEC facility sites to establish a baseline for comparison with induced changes and improve spatial planning of cumulative environmental effects (Aresti et al., 2023; Comfort & Vega, 2011; Hammar et al., 2017). Ongoing monitoring is then required identify any resulting changes from baseline conditions. Appropriate containment along with leak detection and emergency isolation of working fluids requires engineering assessment to establish safe conditions for operation.

4 Conclusions

Limiting future warming to the Paris Agreement targets will likely require large-scale deployment of negative-emission technologies powered by low-carbon energy sources. Coupled Ocean Thermal Energy Conversion (OTEC) and Direct Air Carbon Capture and Storage (DACCS) systems represent one potential pathway for achieving net-negative emissions while simultaneously enabling offshore geological CO_2 sequestration. In this study, offshore depleted oil and gas fields, saline aquifers, and basalt formations were identified as suitable long-term storage reservoirs. In total, 120 reservoirs were found to support coupled OTEC deployment and CO_2 sequestration, with the most favourable conditions occurring above

the Ontong Java Plateau in the equatorial Pacific Ocean, where vertical ocean thermal gradients are greatest. While construction rates, offshore logistics, ecological assessment, and storage readiness remain to be determined, the physical-resource potential of the identified sites implies significant offshore CO_2 sequestration potential exists.

The UVic ESCM provided a physically consistent framework for estimating the cumulative CO_2 emissions associated with the 1.5°C and 2.0°C GMSAT thresholds under a range of future emissions pathways and TCRE values. Across all scenarios, the OTEC power production required to remain below the temperature thresholds increased systematically with increasing TCRE, increasing cumulative emissions, and shorter mitigation timelines. Little additional deployment was required under RCP 2.6, which already assumes substantial negative emissions. Under RCPs 4.5 and 6.0, however, current OTEC and DACCS technology was generally insufficient to prevent surpassing the 1.5°C threshold by 2100, although remaining below this threshold became more feasible under longer timelines extending to 2300 and 2500. Remaining below the 2.0°C threshold was achievable under several RCP 4.5 and 6.0 scenarios, particularly when mitigation timelines were extended. In contrast, neither threshold could be achieved under RCP 8.5 using present-day DACCS energy requirements.

The highest-confidence results were associated with simulations using a TCRE value of 2.0°C per 1000 PgC, consistent with the effective TCRE of the UVic ESCM. Because OTEC efficiency depends directly on the modelled climate response to emissions, uncertainty in required deployment, sequestration capacity, and total cost increased as assumed TCRE values diverged from the model's effective response.

Estimated deployment costs remained extremely large, ranging from approximately 50–66 trillion USD_{2025} under RCP 4.5 and 150–180 trillion USD_{2025} under RCP 6.0, depending on the mitigation timeline. DACCS implementation costs dominated the overall economic burden. Nevertheless, coupled OTEC and DACCS systems possess several important advantages: they can generate their required energy on site or nearby, potentially reduce long-distance CO_2 transport, and operate without direct CO_2 emissions. The principal limitation remains the scale and cost of deployment.

Global temperatures continue to approach and, in some periods, temporarily exceed the Paris Agreement 1.5°C target. Rapid reductions in fossil-fuel emissions, therefore, remain the central requirement for climate stabilization. However, this study suggests that coupled OTEC and DACCS deployment could become a useful component of future mitigation portfolios, particularly under moderate-emission pathways and in scenarios where DACCS efficiency improves substantially. Finally, OTEC uses excess heat accumulated in the ocean from global warming to capture and sequester the anthropogenic carbon dioxide that caused the global warming in the first place. The added benefit of the OTEC/DACCS approach to climate mitigation is that it addresses both historical emissions as well as historical increases in surface temperature.

Declarations

Contributions

L.M., M.E and A.J.W. conceived the research, analysed model results and wrote the paper. L.M. undertook the experiments with the UVic ESCM.

Competing interests

The authors declare no competing interests.

Funding

This research was supported by a Natural Sciences and Engineering Research Council of Canada (NSERC) Discovery Grant awarded to AJW.

Author Contribution

L.M, M.E., and A.W worked on all aspects of this manuscript collaboratively.

Data Availability

The UVic ESCM is publicly available at http://terra.seos.uvic.ca/model/

References

1. Aresti L, Christodoulides P, Michailides C, and Onoufriou T. 2023. Reviewing the energy, environment, and economy prospects of Ocean Thermal Energy Conversion (OTEC) systems. Sustainable Energy Technologies and Assessments, 60(103459). https://doi.org/10.1016/j.seta.2023.103459.
2. https://doi.org/10.1016/j.earscirev.2023.104672.
3. Eby M, Zickfeld K, Montenegro A, Archer D, Meissner KJ, and Weaver AJ. 2009. Lifetime of Anthropogenic Climate Change: Millennial Time Scales of Potential CO2 and Surface Temperature Perturbations. Journal of Climate, 22: 2501–2511. https://doi.org/10.1175/2008JCLI2554.1.
4. Eby M, Weaver AJ, Alexander K, Zickfeld K, Abe-Ouchi A, Cimatoribus AA, et al. 2013. Historical and idealized climate model experiments: an intercomparison of Earth system models of intermediate complexity. Climate of the Past, 9(3): 1111–1140. https://doi.org/10.5194/cp-9-1111-2013.
5. Fanning AF and Weaver AJ. 1996. An atmospheric energy-moisture balance model: climatology, interpentadal climate change, and coupling to an ocean general circulation model. Journal of Geophysical Research: Atmospheres, 101(D10): 15111–15128. https://doi.org/10.1029/96JD01017.

6. Friedlingstein P, O'Sullivan M, Jones MW, Andrew RM, Hauck J, Landschützer P, et al. 2025. Global Carbon Budget 2024. Earth System Science Data, 17(3): 965–1039. https://doi.org/10.5194/essd-17-965-2025.
7. Goldberg D and Slagle AL. 2009. A global assessment of deep-sea basalt sites for carbon sequestration. Energy Procedia, 1(1): 3675–3682. https://doi.org/10.1016/j.egypro.2009.02.165.
8. Gregory JM, Jones CD, Cadule P, and Friedlingstein P. 2009. Quantifying Carbon Cycle Feedbacks. Journal of Climate, 22: 5232–5250. https://doi.org/10.1175/2009JCLI2949.1.
9. International Energy Agency (IEA). 2022. Direct Air Capture: A Key Technology for Net Zero. Organisation for Economic Co-operation and Development. 10.1787/bbd20707-en.
10. IPCC. 2018. Global Warming of 1.5°C. An IPCC Special Report on the impacts of global warming of 1.5°C above pre-industrial levels and related global greenhouse gas emission pathways, in the context of strengthening the global response to the threat of climate change, sustainable development, and efforts to eradicate poverty. Edited by Masson-Delmotte V, Zhai P, Pörtner HO, Roberts D, Skea J, Shukla PR, Pirani A, Moufouma-Okia W, Péan C, Pidcock R, Connors S, Matthews JBR, Chen Y, Zhou X, Gomis MI, Lonnoy E, Maycock T, Tignor M, and Waterfield T. Cambridge University Press, Cambridge, UK and New York, NY, USA. 616 pp. 10.1017/9781009157940.
11. IPCC. 2021. Climate Change 2021: The Physical Science Basis. Working Group I Contribution to the Sixth Assessment Report of the Intergovernmental Panel on Climate Change. Edited by Masson-Delmotte V, Zhai P, Pirani A, Connors SL, Péan C, Berger S, Caud N, Chen Y, Goldfarb L, Gomis MI, Huang M, Leitzell K, Lonnoy E, Matthews JBR, Maycock TK, Waterfield T, Yelekçi O, Yu R, and Zhou B. Cambridge University Press, Cambridge, UK and New York, NY, USA. 10.1017/9781009157896.
12. IPCC. 2023. Climate Change 2023: Synthesis Report. Contribution of Working Groups I, II and III to the Sixth Assessment Report of the Intergovernmental Panel on Climate Change. Edited by Lee H and Romero J. Geneva, Switzerland, 184 pp. 10.59327/IPCC/AR6-9789291691647
13. Jones CD and Friedlingstein P. 2020. Quantifying process-level uncertainty contributions to TCRE and carbon budgets for meeting Paris Agreement climate targets. Environmental Research Letters, 15(7). https://doi.org/10.1088/1748-9326/ab858a.
14. Katavouta A, Williams RG, Goodwin P, and Roussenov V. 2018. Reconciling atmospheric and oceanic views of the Transient Climate Response to Emissions. Geophysical Research Letters, 45: 6205–6214. https://doi.org/10.1029/2018GL077849.
15. Keith DW, Holmes G, St. Angelo D, and Heidel K. 2018. A Process for Capturing CO2 from the Atmosphere. Joule, 2(8): 1573–1594. https://doi.org/10.1016/j.joule.2018.05.006.
16. Kempener R and Neumann F. 2014. Ocean Thermal Energy Conversion: Technology Brief. International Renewable Energy Agency (IRENA).
17. Langer J, Quist J, and Blok K. 2020. Recent progress in the economics of ocean thermal energy conversion: Critical review and research agenda. Renewable and Sustainable Energy Reviews, 130(109960). https://doi.org/10.1016/j.rser.2020.109960.

18. MacDougall AH and Friedlingstein P. 2015. The Origin and Limits of the Near Proportionality between Climate Warming and Cumulative CO2 Emissions. Journal of Climate, 28: 4217–4230. https://doi.org/10.1175/JCLI-D-14-00036.1.
19. MacDougall AH, Swart NC, and Knutti R. 2017. The Uncertainty in the Transient Climate Response to Cumulative CO2 Emissions Arising from the Uncertainty in Physical Climate Parameters. Journal of Climate, 30: 813–827. https://doi.org/10.1175/JCLI-D-16-0205.1.
20. Maroto-Valer MM. 2010. Developments and Innovation in Carbon Dioxide (CO2) Capture and Storage Technology. 1st edition, Woodhead Publishing, Cambridge, UK. 544p.
21. Matthews HD, Gillett NP, Stott PA, and Zickfeld K. 2009. The proportionality of global warming to cumulative carbon emissions. Nature, 459: 829–832. https://doi.org/10.1038/nature08047.
22. Moffat L. 2026. Offshore Carbon Sequestration using Renewable Ocean Energy as a means to meet the Paris Agreement. M.Sc. thesis, University of Victoria, Victoria, Canada. Muralidharan S. 2012. Assessment of Ocean Thermal Energy Conversion. M.Sc. thesis, Massachusetts Institute of Technology, Cambridge, Massachusetts.
23. Nickoloff AG, Olim ST, Eby M, and Weaver AJ. 2025a. An assessment of ocean thermal energy conversion resources and climate change mitigation potential. Climatic Change, 178(103). https://doi.org/10.1007/s10584-025-03933-4.
24. Nickoloff AG, Olim ST, Eby M, and Weaver AJ. 2025b. Environmental impacts from the widespread implementation of ocean thermal energy conversion. Climatic Change, 178(102). https://doi.org/10.1007/s10584-025-03944-1.
25. Nihous GC. 2007. A Preliminary Assessment of Ocean Thermal Energy Conversion Resources. Journal of Energy Resources Technology, 129(1): 10–17. https://doi.org/10.1115/1.2424965.
26. Ocean Energy System. 2021. White Paper on Ocean Thermal Energy Conversion (OTEC). International Energy Agency (IEA) Technology Programme for Ocean Energy Systems.
27. Oil & Gas Climate Initiative. 2023. CO_2 Storage Resource Catalogue – CCUS projects, Cycle 4.
28. Olim ST, Nickoloff A, Moffat LM, Weaver AJ, and Eby M. 2025. Mitigating anthropogenic climate change with aqueous green energy. Scientific Reports, 15(1700). https://doi.org/10.1038/s41598-025-86042-7.
29. Pacanowski RC. 1996. MOM 2 documentation user's guide and reference manual. Geophysical Fluid Dynamics Laboratory/NOAA Ocean Technical Report 3.2, Princeton, NJ. 232p.
30. Planke S, Bellwald B, Millett J, Planke EEE, Zastrozhnov Z, Carlevaris P, et al. 2021. Permanent Carbon Sequestration Potential in Offshore Basalt Sequences on the NW European Continental Margins. *In* Proceedings of the 82nd European Association of Geoscientists & Engineers Annual Conference & Exhibition, Amsterdam, The Netherlands, 18–21 October 2021. pp. 1–5. https://doi.org/10.3997/2214-4609.202011841.
31. Rajagopalan K and Nihous GC. 2013. Estimates of global Ocean Thermal Energy Conversion (OTEC) resources using an ocean general circulation model. Renewable Energy, 50: 532–540. https://doi.org/10.1016/j.renene.2012.07.014.

32. Ricke KL and Caldeira K. 2014. Maximum warming occurs about one decade after a carbon dioxide emission. Environmental Research Letters, 9(12). https://doi.org/10.1088/1748-9326/9/12/124002.
33. Rocheleau GJ and Grandelli P. 2011. Physical and biological modeling of a 100 megawatt Ocean Thermal Energy Conversion discharge plume. *In* Proceedings of the OCEANS'11 MTS/IEEE KONA, 19–22 September 2011. pp. 1–10. https://doi.org/10.23919/OCEANS.2011.6107077.
34. Rodríguez Buño M. 2013. Near and Far Field Models of External Fluid Mechanics of Ocean Thermal Energy Conversion (OTEC) Power Plants. M.Sc. thesis, Massachusetts Institute of Technology, Cambridge, Massachusetts.
35. Seshadri AK. 2017. Origin of path independence between cumulative CO2 emissions and global warming. Climate Dynamics, 49: 3383–3401. https://doi.org/10.1007/s00382-016-3519-3.
36. Shen W, Chen X, Qiu J, Hayward JA, Sayeef S, Osman P, Meng K, and Dong ZY. 2020. A comprehensive review of variable renewable energy levelized cost of electricity. Renewable and Sustainable Energy Reviews, 133(110301). https://doi.org/10.1016/j.rser.2020.110301.
37. Weaver AJ. 2008. Keeping our Cool: Canada in a Warming World. Viking Canada, Toronto, Ontario, ISBN:978-0-670-06800-5, 323pp.
38. Weaver AJ, Eby M, Wiebe EC, Bitz CM, Duffy PB, Ewen TL, et al. 2001. The UVic earth system climate model: Model description, climatology, and applications to past, present and future climates. Atmosphere-Ocean, 39(4): 361–428. https://doi.org/10.1080/07055900.2001.9649686.
39. World Meteorological Organization. 2025. State of the Global Climate 2024. World Meteorological Organization, Geneva, Switzerland, WMO-No.1368
40. Zickfeld K and Herrington T. 2015. The time lag between a carbon dioxide emission and maximum warming increases with the size of the emission. Environmental Research Letters, 10(031001). https://doi.org/10.1088/1748-9326/10/3/031001.
41. Zickfeld K, Eby M, Matthews HD, and Weaver AJ. 2009. Setting cumulative emissions targets to reduce the risk of dangerous climate change. Proceedings of the National Academy of Sciences, 106(38): 16129–16134. https://doi.org/10.1073/pnas.0805800106.
42. Zickfeld K, Eby M, Weaver AJ, Alexander K, Crespin E, Edwards NR, et al. 2013. Long-Term Climate Change Commitment and Reversibility: An EMIC Intercomparison. Journal of Climate, 26(16): 5782–5809. https://doi.org/10.1175/JCLI-D-12-00584.1.

Figures

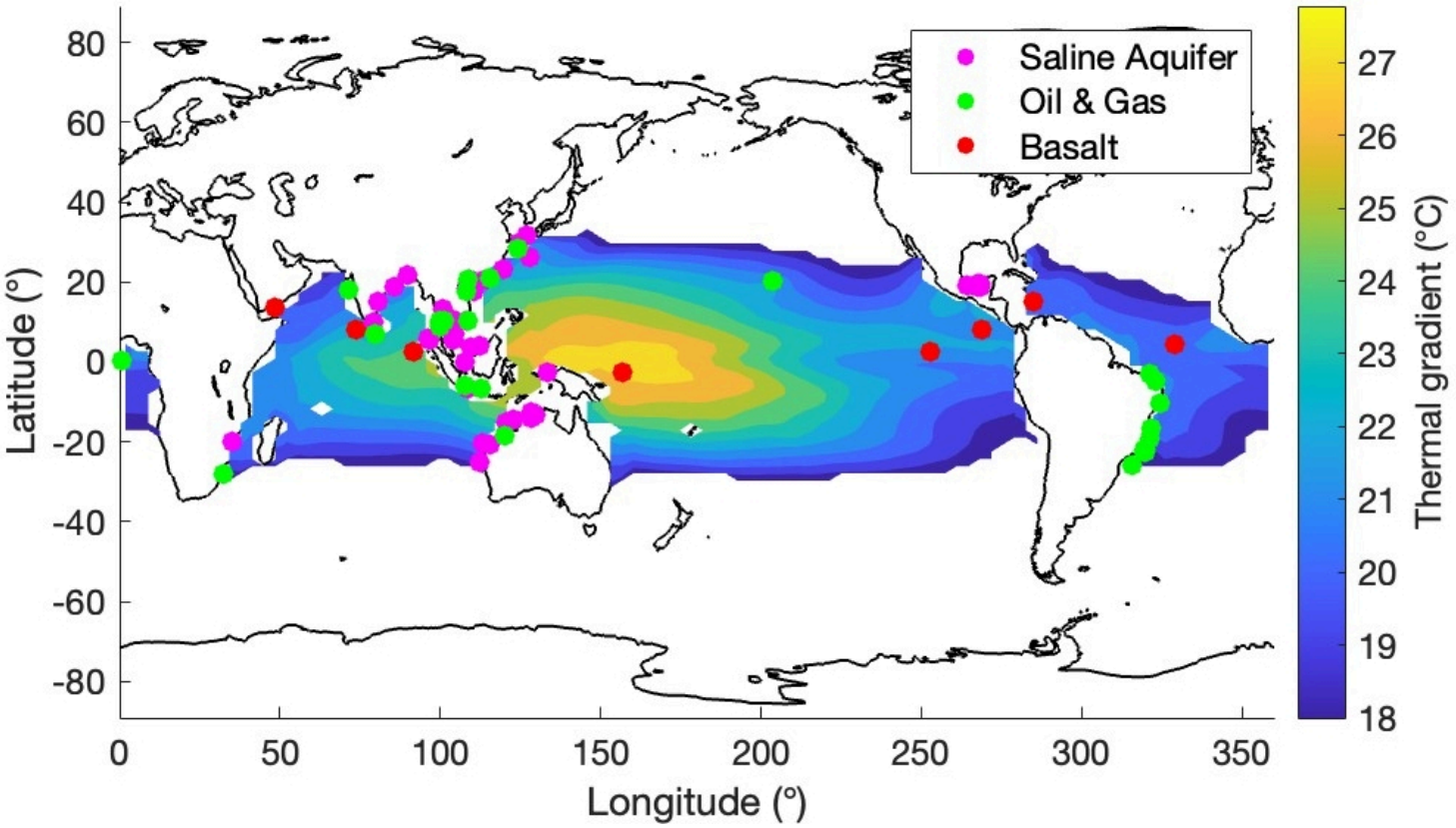


Figure 1

Map identifying the potential OTEC/DACCS deployment sites. The region with an adequate thermal gradient of 18°C or greater is also contoured. Potential carbon sequestration reservoirs are indicated by dots: saline aquifers (purple); depleted oil and gas fields (green); and basalt formation regions (red). Sites across all categories of water depths are included. The region with an adequate thermal gradient of 18°C or greater is represented as a contour plot.

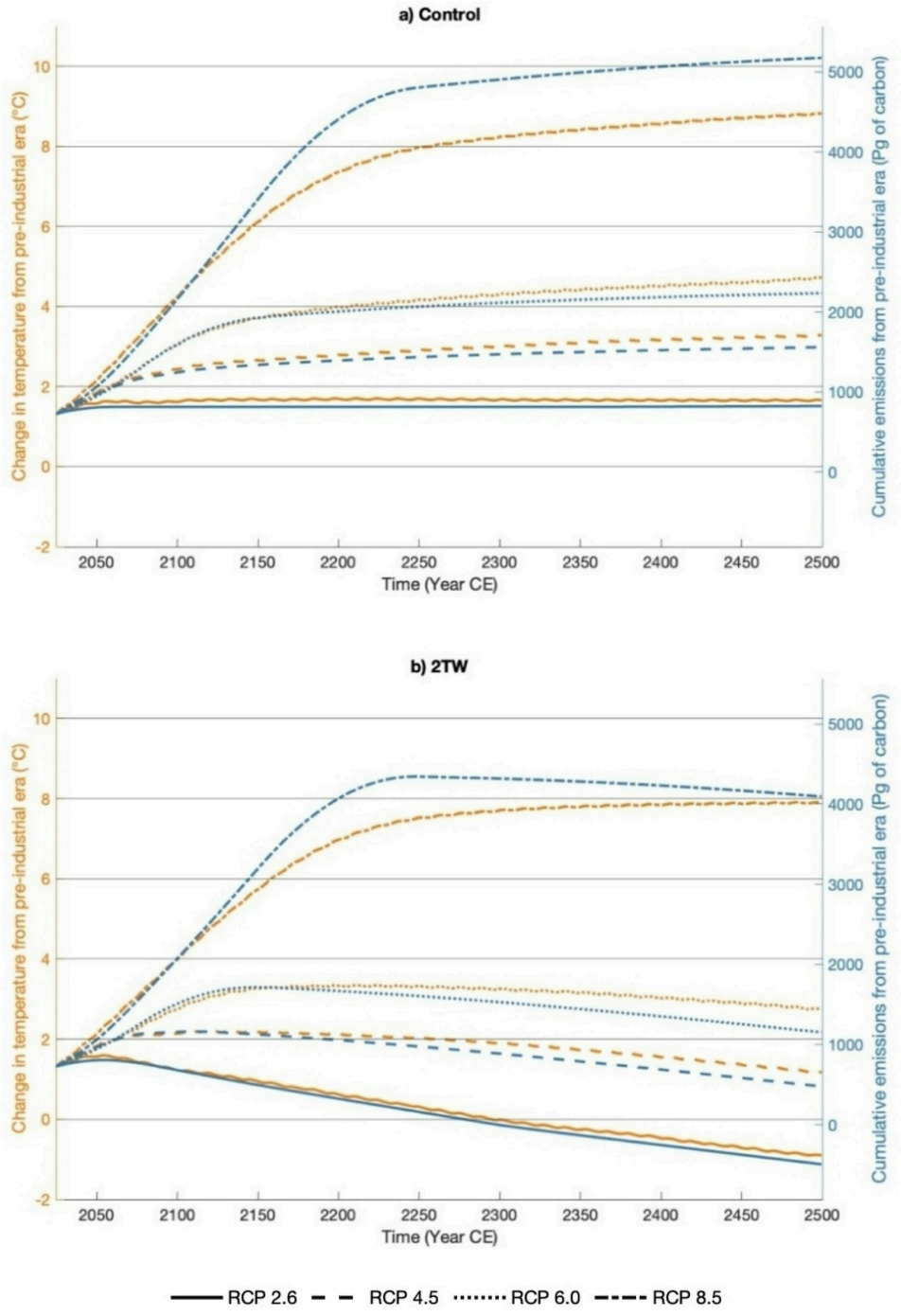


Figure 2

Year 2025 to year 2500 change in GMSAT (°C; orange) and cumulative emissions (PgC; blue) since the pre-industrial era. Trajectories are shown for integrations under RCP 2.6 (solid), RCP 4.5 (dashed), RCP 6.0 (dotted), and RCP 8.5 (dash-dotted). Horizontal black lines represent the observed offset between the change in GMSAT and cumulative emissions from the pre-industrial era to the year 2025 (Friedlingstein et al. 2025; World Meteorological Organization 2025). **a)** trajectories for control scenarios

without coupled OTEC and DACCS deployment; **b)** trajectories for integrations with 2 TW of target peak power production and the OTEC-HIGH condition for sequestration energy. Vertical axes are scaled to represent a TCRE value of 2.0°C per 1000 PgC.

Supplementary Files

This is a list of supplementary files associated with this preprint. Click to download.

- OTECSupplementary.docx